



Error introduced by direct 3D printing of compression samples of PLA made by FDM process

Silvia Ilaria Scipioni¹ · Francesco Lambiase¹

Received: 31 July 2023 / Accepted: 27 October 2023 / Published online: 7 November 2023
© The Author(s) 2023

Abstract

This study delves into the crucial aspect of sample preparation methodology and its profound impact on characterizing the physical and mechanical properties of components fabricated through the material extrusion (fused deposition modeling—FDM) process. Two distinct manufacturing approaches, direct printing and sample extraction from a plate, were employed to produce samples. To assess the influence of artifacts introduced by direct printing, compression tests were conducted under various loading directions. The investigation extends to density measurements and comprehensive morphological analysis, which plays a pivotal role in understanding the ramifications of different manufacturing approaches and principal sample directions. Notably, the research findings reveal that direct printing inflicts significant artifacts within the samples, fundamentally altering the properties obtained during testing. These artifacts substantially affect density measurements and mechanical behavior, indicating a potential avenue for future research and applications. Besides, the printing direction also significantly influenced the extent of the artifacts and differences in mechanical behavior. The maximum difference in density measurement was -5.3% , while Young's modulus reached -29% , and yield strength ranged between -12% (for vertical samples) and $+18\%$ for horizontal samples with filaments arranged along the loading path. These findings underscore the necessity for meticulously crafted quality assessment protocols when utilizing functional parts manufactured through the material extrusion process. Such protocols should also consider the influence of sample dimensions on the mechanical characteristics of the components.

Keywords Additive manufacturing · Fused deposition modeling · Characterization · Material extrusion

1 Introduction

Additive manufacturing (AM) processes are having an increasing impact on the manufacturing sector. Since its early acceptance for rapid prototyping, additive manufacturing (AM) has gradually expanded to include new applications like rapid tooling and the production of highly personalized items. This is because adopting these technologies has intrinsic advantages in additive manufacturing. These include distributed production, high levels of customization, minimal fixed costs, very inexpensive machining, speedy setup times, and reduced logistic costs [1–3]. The creation of novel materials, even those with functionalized

fillers, and machines with greater accuracy and high-temperature heating chambers (techno-polymers such as polyether ether ketone (PEEK) [4–9], polyethylenimine (PEI) [10–16], polyaryletherketone (PAEK) [17, 18], as well as reinforced plastics field [19–25]) provides new opportunities and answers to manufacturing's demands. However, certain issues that are specifically related to the layer-by-layer deposition approach still afflict AM components. Internal voids, surface finishing, distortion, and porosities are widespread in various additive manufacturing techniques [26].

Material extrusion (MatExt), one of the AM techniques, is the method most frequently employed to create polymeric components. It is possible to embed functionalized fillers for structural purposes (like glass or carbon fibers) or to produce electrically conductive material, thanks to the machine's simplicity, ease of scalability, great material availability, reduced material cost (especially when compared to polymeric powders used in selective laser sintering), and availability of materials (such as copper or even graphene).

✉ Francesco Lambiase
francesco.lambiase@univaq.it

¹ Department of Industrial and Information Engineering and Economics, University of L'Aquila, Via G. Gronchi 18, Zona Industriale Di Pile, 67100 L'Aquila, AQ, Italy

Because of the material's viscosity during deposition, items created with the MatExt technique suffer from the existence of voids. The viscosity increases quickly after the extrusion when the material comes into contact with the underlying layer. This severely restricts the degree of healing and limits the contact interface between overlapping layers [27]. Since there are inner voids and a sintering process is used to adhere the layers together rather than welding, the resulting mechanical behavior is considerably different from that of plastic components made using conventional techniques, such as injection molding. This is also the case for semicrystalline materials since the crystallization kinetics may prevent the healing of neighboring deposited filaments [28–32].

Although AM processes enable the direct production of a sample without further work, direct sample printing may cause some artifacts while determining the mechanical behavior of AM components. Indeed, the mechanical behavior of these components, while keeping constant the material and other process conditions, is affected by the thermal history, which greatly influences the adhesion of consecutive layers. The thermal history influences the degree of healing [27]. Consequently, interlayer bonding is strongly affected by all the printing parameters that influence the thermal history, such as the nozzle temperature, the nozzle speed, the layer thickness, the printing strategy, and the degree of filling. In addition, the thermal history also determines the viscosity of the material being deposited; consequently, it also strongly influences the effective bonding area between the filaments [28, 33] and the voids. With these printing parameters held constant, the interlayer time, referring to the duration between successive extrusion passes at the same point after completing one layer, is solely influenced by the geometry of the deposited layer. The interlayer time serves as a comprehensive indicator, encapsulating the contributions of numerous printing parameters to the interlayer adhesion. Indeed, opting for process parameters that result in extended interlayer times can lead to significant cooling of the printed layer, thereby diminishing adhesion with the subsequent layer. Conversely, excessively short interlayer times may compromise dimensional accuracy since the “substrate material” remains in a rubbery state.

While determining the mechanical behavior of an AM component, direct sample print is widely adopted [34–36]. The sample with all its features (e.g., dogbane for tensile tests) is produced. However, this sample may show different behavior as compared to that of a larger component since the interlayer time could be highly different. Different interlayer times elapsed when using series or parallel deposition strategy. This indicates that the interlayer time should be similar between the effective workpiece and the sample printing. Another potential artifact that can occur during direct printing of a sample is related to the effective deposition speed. In cases where small samples are being

produced, despite configuring the same nominal deposition rate, the acceleration and deceleration phases may impede reaching the intended nominal speed due to the limited length of the sample. Consequently, this can result in disparities between the properties of a sample generated through direct printing and one that is “as extracted” from a component.

Finally, as reported by several studies [37, 38], the mechanical behavior of printed samples is also sensitive to the distance from the building plate. In the MatExt process [6–8, 10, 39], layers in contact with the building plate show higher density than overlying layers. In addition, as the building plate is typically kept at temperatures close or even higher to the polymer's glass transition temperature, aging may occur in these layers. This also alters the mechanical properties of these layers compared to those of the rest of the sample [37].

Mechanical characterization tests are conducted to assess the physical and mechanical properties of materials or components. The main scope of these tests is to determine how a material or structure responds to various types of mechanical forces and to gather data for design, quality control, and safety purposes. The tests are performed on samples whose characteristics are representative of the whole component. Typically, the samples used for mechanical tests are extracted (cut or milled, depending on the shape) from the component. On the other hand, since AM processes enable the production of very complex geometries, the mechanical characterization of the samples has been largely performed by directly printing the sample with the final geometry. Neither of the previous studies analyzed whether or not the samples directly printed show the same behavior as those produced by “extraction” from a larger component. Indeed, the “deposition history” and particularly the thermal history can be significantly different from that occurring during the production of a real (larger) component. Thus, direct sample printing may introduce artifacts that can lead to significant differences in the mechanical properties of the sample as compared to those of a larger component. The different deposition histories may lead to underestimation or overestimation of the physical properties (e.g., density) and mechanical properties. On the other hand, the “classical” sample preparation, through sample cutting or milling from a larger component, demands more effort for sample production and is more time-consuming.

The primary objective of this study is to assess the extent to which the mechanical and physical properties of samples are influenced by the sample manufacturing strategy, specifically the sample manufacturing protocol. To this end, two distinct approaches were followed:

- 1) Direct sample printing: In this widely adopted approach, samples were printed directly at their final dimensions.

- 2) Sample extraction: The second approach involved manufacturing larger components (plates) from which samples were subsequently extracted to attain the desired final dimensions.

A comparative analysis of compression samples was performed for several reasons. First, straight samples are relatively easier to cut, making them suitable for this investigation. Additionally, understanding compressive behavior is crucial for the adoption of the material extrusion (MatExt) process in applications such as rapid tooling [40], where components like molds and dies are often subjected to autoclave cycles. As many previous studies have indicated, the mechanical performance of components can be influenced by their distance from the building plate during the printing process. This effect can vary between samples printed vertically and horizontally [41]. Consequently, we prepared compression samples oriented in different loading directions using both of the aforementioned manufacturing protocols. We conducted a comprehensive examination of physical properties, including density and inner void dimensions, followed by compression tests to determine essential mechanical properties such as elastic modulus and yield strength. Additionally, we conducted thermal analysis during the sample printing process to gain insights into the impact of sample dimensions on thermal history, thereby shedding light on their physical and mechanical properties.

2 Materials and methods

2.1 Sample production

Poly lactide acid (PLA), supplied by RS PRO, was used in the study. The filament had an initial diameter of $1.75 \text{ mm} \pm 0.05 \text{ mm}$. Compression tests were performed using a sample with a box geometry with a square base having a side of 12 mm and a height of 48 mm. A schematic of the sample is reported in Fig. 1.

The samples were produced on a commercial Creality machine, model Ender 6. Table 1 provides an overview of the primary deposition circumstances. A large part of these parameters show a direct influence on the interlayer bonding behaviors [42, 43], as well as other characteristics such as surface roughness and dimensional accuracy. Indeed, the nozzle temperature, the layer thickness, the building plate temperature, as well as the extrusion multiplier, and the infill percentage directly influence the thermal history that determines the interlayer bonding of subsequent layers. Furthermore, the layer's dimensions, which represent the cross-section of the component being printed, also play a crucial role in influencing interlayer bonding. This is because they, along with the nozzle speed, dictate the interlayer time.

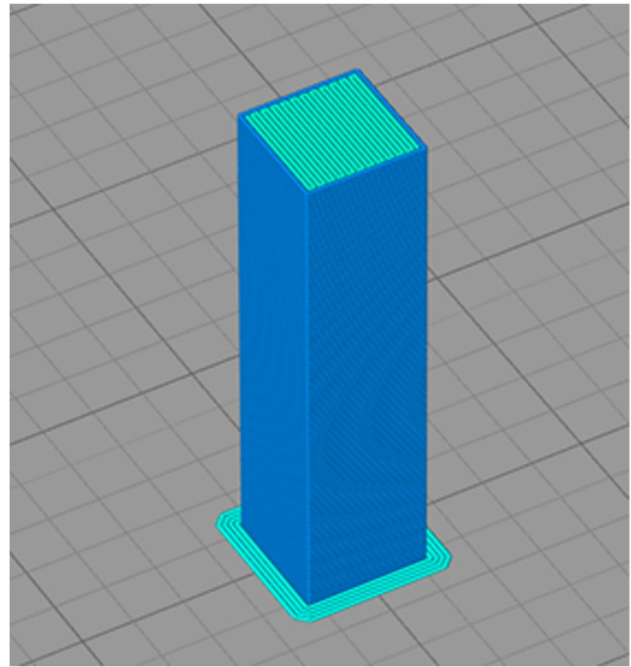


Fig. 1 Schematic of the sample produced with the selected deposition strategy

Table 1 Main deposition conditions

Process parameter	Value
Nozzle temperature [°C]	210
Building plate temperature [°C]	60
Nozzle speed [mm/min]	4000
Nozzle diameter [mm]	0.4
Extrusion width [mm]	0.5
Layer thickness [mm]	0.2
Infill percentage [%]	100
Infill strategy	Rectilinear
Number of external shells	1
Extrusion multiplier	100%

The following reference explains the effects of six parameters on strength (PLA material) and can be used for the parameter selection constant values [44].

Three different orientations were tested, leading to (1) vertical samples (the loading direction corresponds to the material extrusion machine Z-axis), (2) horizontal samples with filaments arranged transverse to the loading direction, and (3) horizontal samples with filaments arranged parallel to the loading direction. The samples were produced using two different approaches: direct printing and sample extraction (cut) from larger components (plate).

The final dimensions of the samples used for compression tests were $12 \text{ mm} \times 12 \text{ mm} \times 48 \text{ mm}$. Such values are

similar to those reported by the ASTM D695, which reports that for the evaluation of the Young's modulus and the offset yield stress the height should be four times the side ($12.7 \times 12.7 \times 50.8$ mm). Such dimensions were also adopted to let the samples to better fit the experimental devices.

The samples were produced using the direct printing approach with the final dimension ($12 \text{ mm} \times 12 \text{ mm} \times 48 \text{ mm}$). The printing and cutting involved more effort for sample preparations. Indeed, a plate with dimensions of $12 \text{ mm} \times 130 \text{ mm} \times 60 \text{ mm}$ was produced. From this plate, four samples for each direction were made. The side regions of the plate were cut to avoid embedding regions where acceleration/deceleration and inversion of deposition direction into the samples. To this end, a water-cooled saw blade was adopted for the cuts. To understand the adopted approach, a plate layout with the cuts is reported in Fig. 2. The picture shows that configurations V1, H1, and HL1 immediately produce the samples. However, some of these samples (especially those of type H1 and HL1) are in contact with the building platform. Thus, such regions could be affected by prolonged contact with the building platform, which may alter the region's structure and mechanical properties, as reported in [37]. On the other hand, V2 and H2 samples are cut from the 3D-printed plaque, taking care to avoid the region coming in contact with the building plate. H3 and H4 samples (shown in Fig. 2d) were produced with benchmarking purposes to determine the influence of the printed part size on the mechanical behavior.

2.2 Thermal analysis

The mechanical characteristics of samples manufactured using the MatExt process are intricately linked to the material viscosity and the bonding that occurs between filaments through interdiffusion. Consequently, thermal analysis was conducted to discern how sample dimensions influence their thermal history. Furthermore, the local temperature measurements were analyzed to investigate the potential development of edge effects during the printing process, which could impact sample characteristics.

Thus, an infrared camera, model E60 by Flir, was involved during the MatExt process to capture temperature distributions and variations in real time. The methodology closely followed that described by Bartolai et al. [45], where the thermal camera was positioned alongside the specimen to record the thermal cycles imposed during printing. This configuration is visually depicted in Fig. 3. To ensure high-quality data capture, the highest available acquisition frequency (30 Hz) was selected as the deposition time for manufacturing the entire specimen extended up to 7 h. Subsequently, the thermal history was analyzed using the ResearchIR software. As evident from Fig. 3, the thermal camera is securely mounted on the machine frame, allowing for continuous temperature monitoring throughout the entire deposition process.

Three main cases were analyzed to understand the influence of the sample dimension on the temperature history:

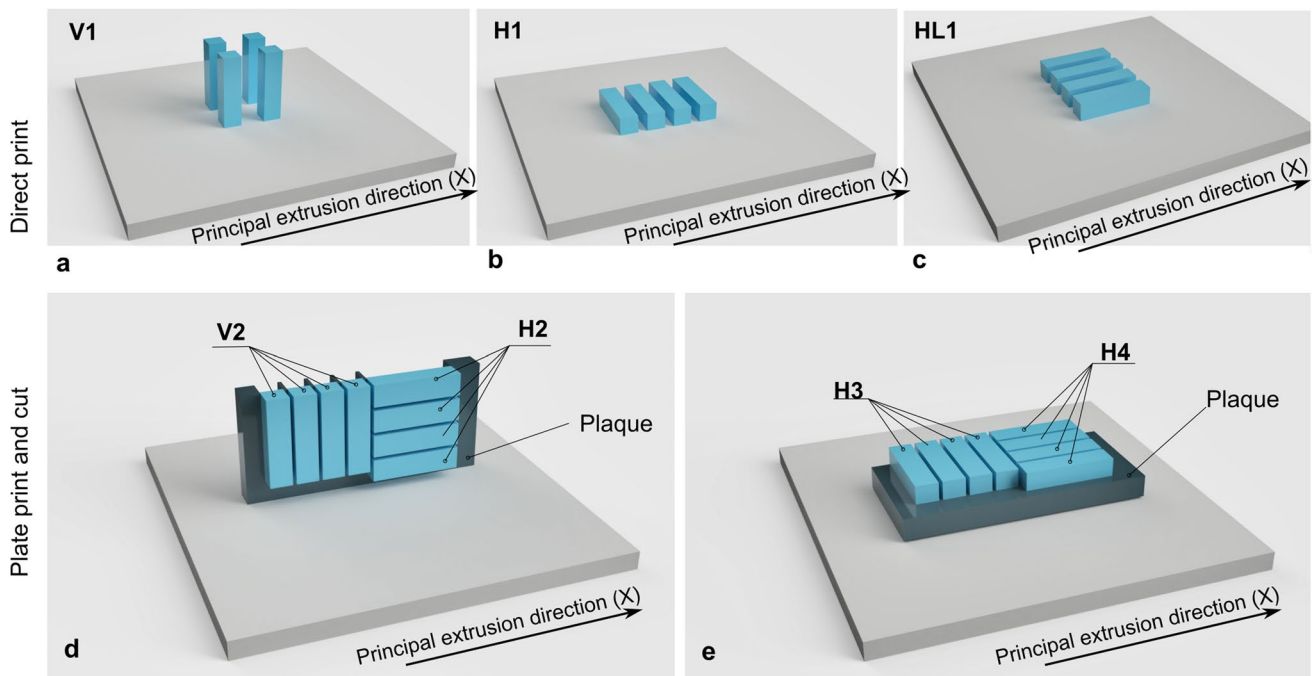


Fig. 2 Schematic of the adopted printing strategies: direct print of **a** vertical, **b** horizontal samples, and **c** horizontal with longitudinal filaments. Plaque print and cut of **d** vertical plaque and **e** horizontal plaque

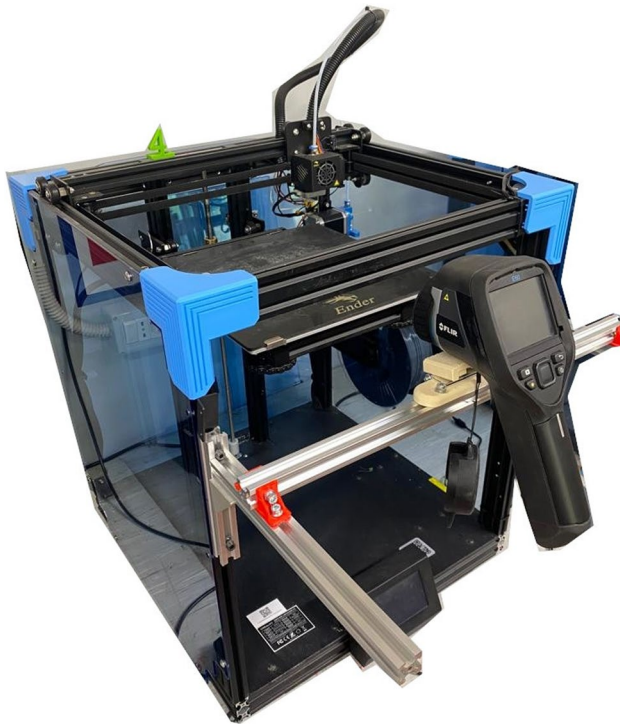


Fig. 3 Picture of the IR thermal measurement during the MatExt process

(1) direct printing of a single (vertical) specimen, (2) direct printing of 4 (vertical samples), and (3) plate printing. This enabled the produce samples with different interlayer times.

2.3 Sample characterization

The samples were geometrically characterized before mechanical tests to establish the component densities. The dimensions were determined using a centesimal micrometer. The weight of the samples was then determined using a Precisa balance model XT1220M. This enabled us to estimate the density of the samples and how the chosen process parameters affected it.

According to ASTM D695 specifications, compression tests were carried out. A load cell with a full scale of 50 kN and a universal testing machine mode C43.50 were used. The tests were conducted using a traverse speed of 1 mm/min. During the tests, the strain of the sample was measured through an extensometer model 632.24F-50 by MTS. The tests were conducted up to a displacement of 2 mm. A picture of the sample during the compression test is reported in Fig. 4.

Table 2 provides an overview of the final experimental strategy.

Optical microscopy was used to better comprehend the materials' morphology before and after the mechanical tests. To accomplish this, a LEICA stereoscope model



Fig. 4 Picture of the sample during the compression test

M205 was used to ascertain the morphology of the upper surface. Additionally, a LEICA DM5000 metallographic microscope was used to comprehend better the microstructural features (interlayer neck and void sizes). Some samples were cross-sectioned and polished using abrasive paper to see better the internal flaws of the samples and the impact of the material flow (up to 2400 grit). Thus, a cooled diamond blade was used to cross-section the samples in the past. The samples were then molded and polished following consolidated metallographic techniques.

3 Results

3.1 Density of the samples

Figure 5 summarizes the density measurements performed on the different samples (green bars highlight the

Table 2 Levels of the full factorial experimental plan

Sample	Manufacturing	Sample direction
V1	Direct print	Vertical
H1	Direct print	Horizontal
HL1	Direct print	Horizontal
V2	Extracted from the vertical plate	Vertical
H2	Extracted from the vertical plate	Horizontal
H3	Extracted from the horizontal plate	Vertical
H4	Extracted from the horizontal plate	Horizontal

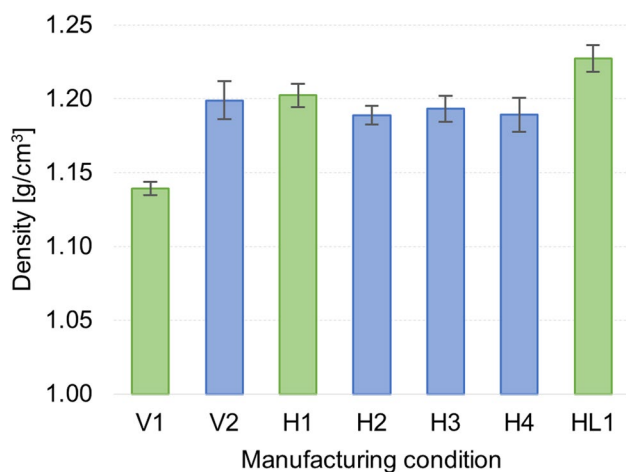


Fig. 5 Influence of the deposition conditions on the density of the samples

measurements performed on directly printed samples). As can be inferred, direct sample printing led to underestimating the density in vertical samples. The density of V1 samples was 5.3% lower than that measured on extracted samples V2. On the other hand, negligible differences (lower than 1%) were found while comparing the density of all the samples extracted from the plaque. This indicates good robustness and reproducibility of the procedure adopted while extracting the samples. Directly printed samples HL1 showed a slightly higher density than the other samples. This difference can be ascribed mainly to the inversion of the printing direction (at the edges). On the other hand, the average density was less affected by the distance of the sample from the building plate. The samples V2 and H2 which were extracted far from the plate showed similar density compared to samples H3 and H4, which were extracted from a plaque printed with a large area in contact with the building (heated) plate.

3.2 Mechanical characteristics

Figure 6 depicts the influence of the printing strategy and direction on Young's modulus. As can be inferred, directly printed samples V1 and H1 showed lower Young's modulus than the corresponding "extracted" samples V2 and H3. The measurements using V1 samples underestimated Young's modulus by 10%. Similarly, the difference between Young's modulus measured along the horizontal direction was even more marked; indeed, for H1, the average Young's modulus was 1380 MPa, while that of the H3 sample was 1780 MPa, corresponding to an underestimation of 29%.

Only direct printed samples HL1 showed a similar Young's modulus as compared to the corresponding "extracted" samples H4 and H2 because, during the compression test, filaments are oriented perpendicular to the

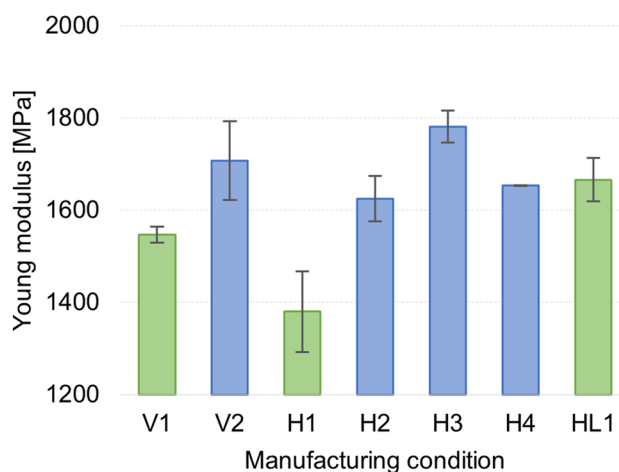


Fig. 6 Influence of the deposition conditions on the Young modulus of the samples

direction of load application in all three specimens considered. Direct printed samples H1 showed the lowest Young's modulus because, during the compression test, these samples were not compressed in the direction of layer growth; indeed, layers were not compressed with each other, but there was compression of filaments (Fig. 7).

Figure 8 depicts the influence of the printing strategy and direction on the yield stress. As can be inferred, directly printed samples V1 showed lower yield stress than the corresponding "extracted" samples V2. The measurements performed using V1 samples underestimated the yield stress by 12%. The difference between the yield stress measured along the horizontal direction was not marked; indeed, for H1, the average yield stress was 61 MPa, while that of the H3 sample was 63 MPa. Differences were more marked if compared to H4 and HL1; HL1 depicts an average yield stress of 73 MPa, corresponding to an underestimation with H2 of 18%. The motivation for this difference can be found in the printing mode, which results in a 3% higher density in HL1 than in H2. HL1, having been printed in the horizontal direction, has a greater contact surface with the printing plane than H2, leading to a higher density.

3.3 Optical microscopy

The specimens with the lowest density are the direct printed vertical samples V1. The average density of the sample V1 is 1.14 g/cm³, while the density of the corresponding "extracted" sample V2 is 1.20 g/cm³, showing an increase for the extracted specimens of 5.3%. Figure 9 shows the porosities present in the two types of specimens analyzed. Figure 7a shows the porosities in the V1 specimens, which are much more evident than those in the V2 specimens, shown in Fig. 7b.

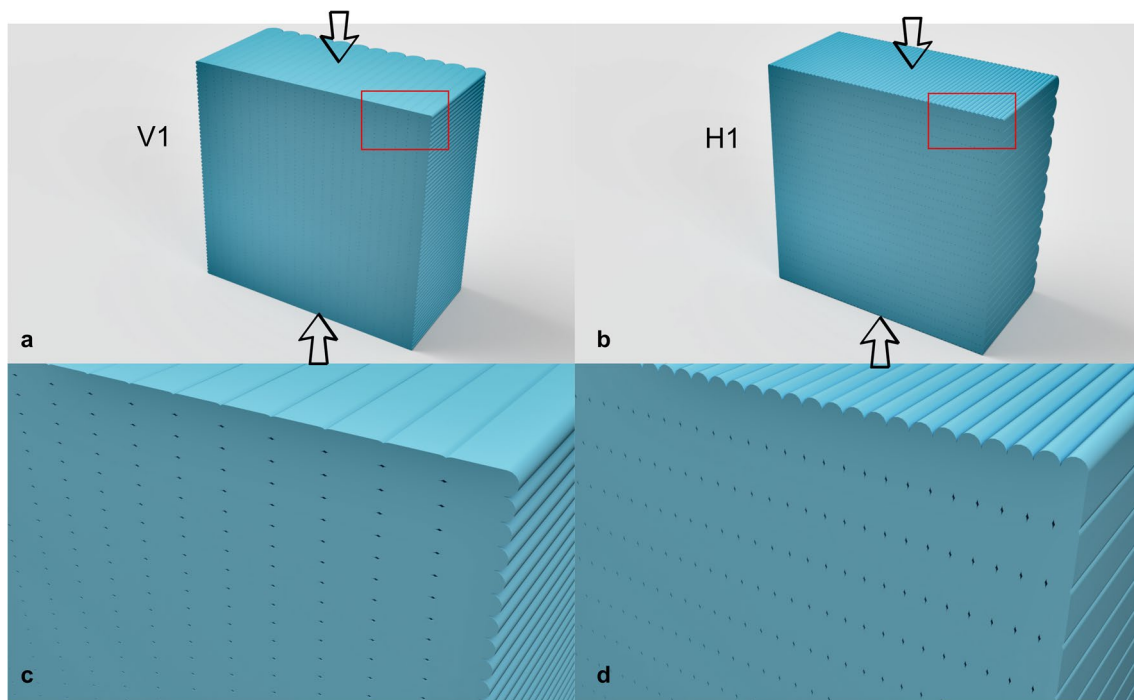


Fig. 7 Schematic of the cross sections performed on V1 samples (a) and H1 samples (b) with a zoom on the direction of the layer during compression test for V1 samples (c) and H1 samples (d)

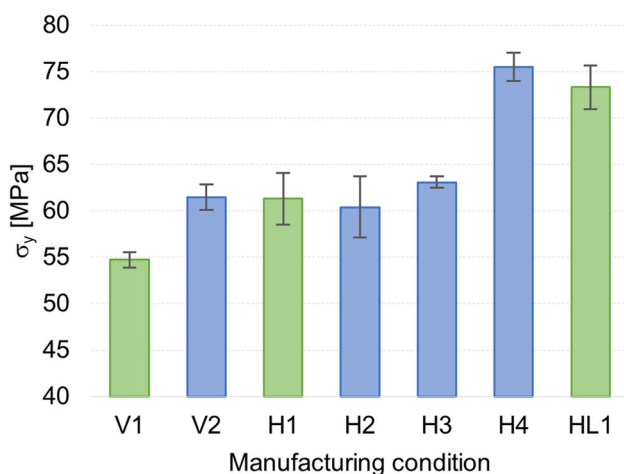


Fig. 8 Influence of the deposition conditions on the yield stress of the samples

Figure 10 shows the porosities present in the H1 samples, which are those directly printed in the horizontal direction. Observing how the porosities present a gradient in their distribution is possible. The lower area, in contact with the printing plane, shows almost absent porosities; while moving away from the printing plane, the porosities gradually increase.

The results from the test matrix are summarized in Table 3.

3.4 Thermal analysis

Figure 11 illustrates thermal infrared (IR) images captured at various stages during the deposition of directly printed samples. The images vividly display temperature variations within the printed structure. Initially, the upper layers exhibit higher temperatures immediately after deposition, reflecting their recent extrusion. However, the temperatures in these upper layers quickly decrease due to heat diffusion toward the underlying layers and heat dissipation into the surroundings through radiation and convection. This rapid cooling results in a substantial drop of approximately 80–90 °C in filament temperature.

In contrast, the first layers, in direct contact with the build platform, maintain a relatively higher temperature, approximately 60 °C, even after an extended period since deposition. This sustained temperature can be attributed to the continuous heat exchange between these layers and the build platform.

The thermal images of the directly printed samples also reveal distinct horizontal temperature gradients. The isotherms exhibit a characteristic parabolic pattern, which arises from increased heat dissipation at the sample corners compared to the sides. This gradient in temperature distribution highlights the complex thermal dynamics within the printed structure.

Fig. 9 Porosities in direct printed vertical samples V1 (a) and in corresponding “extracted” samples (b)

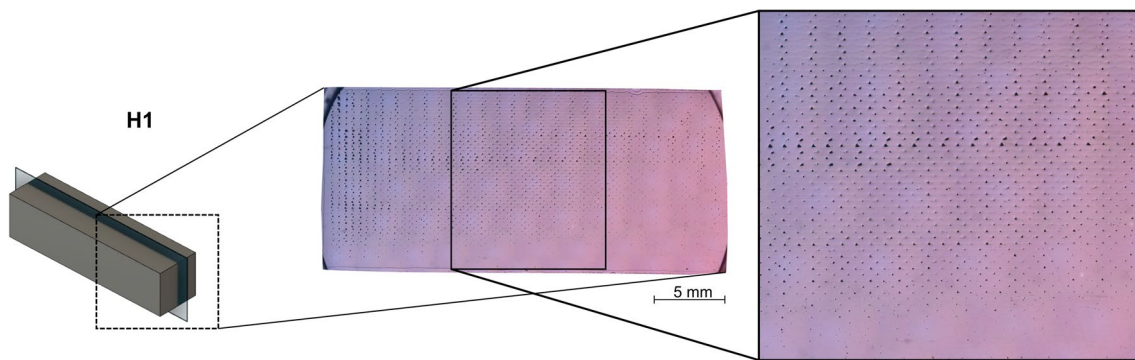
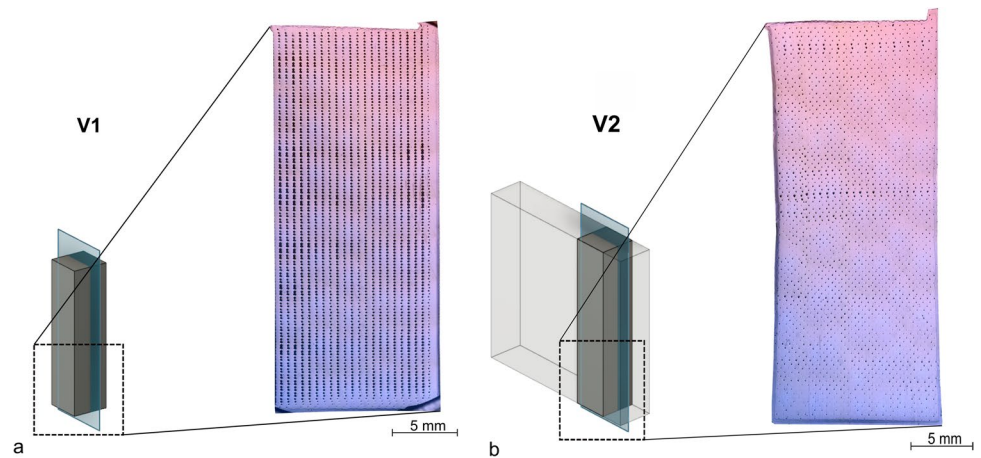


Fig. 10 Porosities in direct printed horizontal samples (H1) with a zoom on their distribution

Table 3 Summary of the results from the test matrix

	Density [g/cm^3]		Young modulus [MPa]		σ_y [MPa]	
	Mean value	Standard deviation	Mean value	Standard deviation	Mean value	Standard deviation
V1	1.139	0.004	1547	17	54.7	0.9
V2	1.199	0.013	1708	85	61.5	1.4
H1	1.202	0.008	1380	88	61.3	2.8
H2	1.189	0.006	1625	49	60.4	3.3
H3	1.193	0.009	1781	35	63.1	0.6
H4	1.189	0.012	1653	1	75.5	1.5
HL1	1.227	0.009	1666	47	73.3	2.3

The sequence of the IR images of the directly printed samples deposited in parallel (four at a time) has been reported in Fig. 12. The IR map indicates a smoother gradient of temperature as compared to that observed during single-sample printing. In addition, the average temperature was much lower. Both these phenomena were addressed to the longer interlayer time that promoted higher heat diffusion and heat loss when four specimens were printed instead of only one.

The thermal infrared (IR) images, as depicted in Fig. 13, distinctly highlight a contrasting thermal distribution pattern measured on the plate. Notably, a considerably steeper temperature gradient is observed in the vertical direction, particularly just beneath the deposited layer. This gradient is a consequence of the significantly longer interlayer time, which is directly proportional to the layer's surface area. In contrast, these images reveal negligible horizontal temperature gradients within the printed structure.

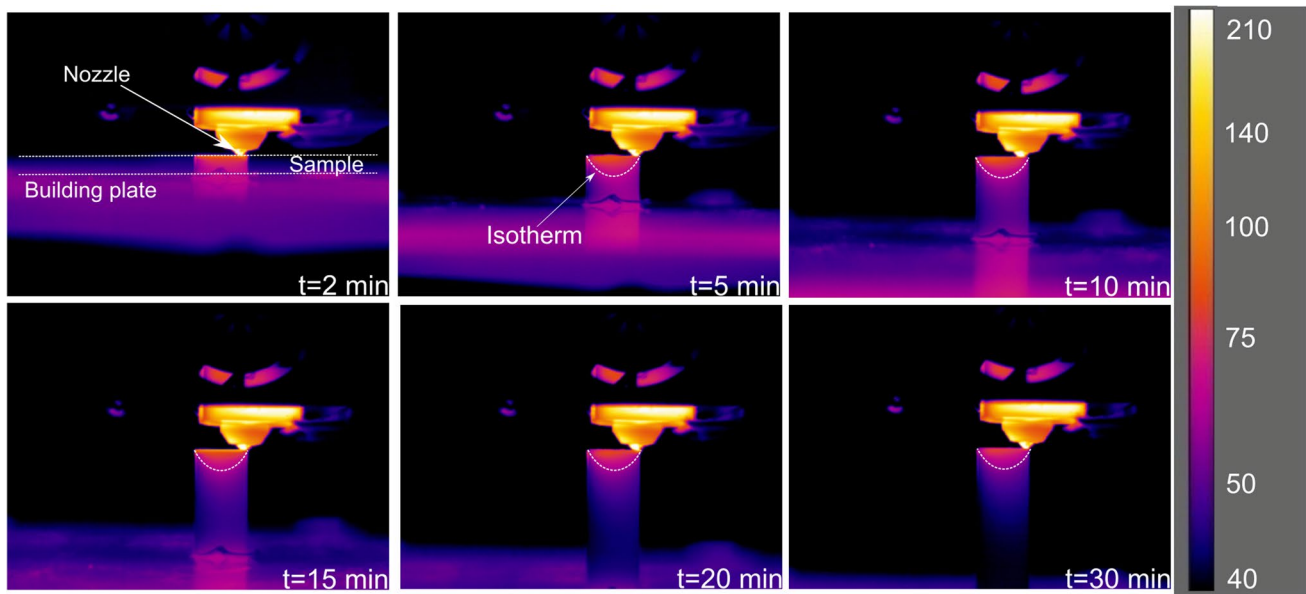


Fig. 11 IR maps recorded at different deposition times during 3D printing of a single sample

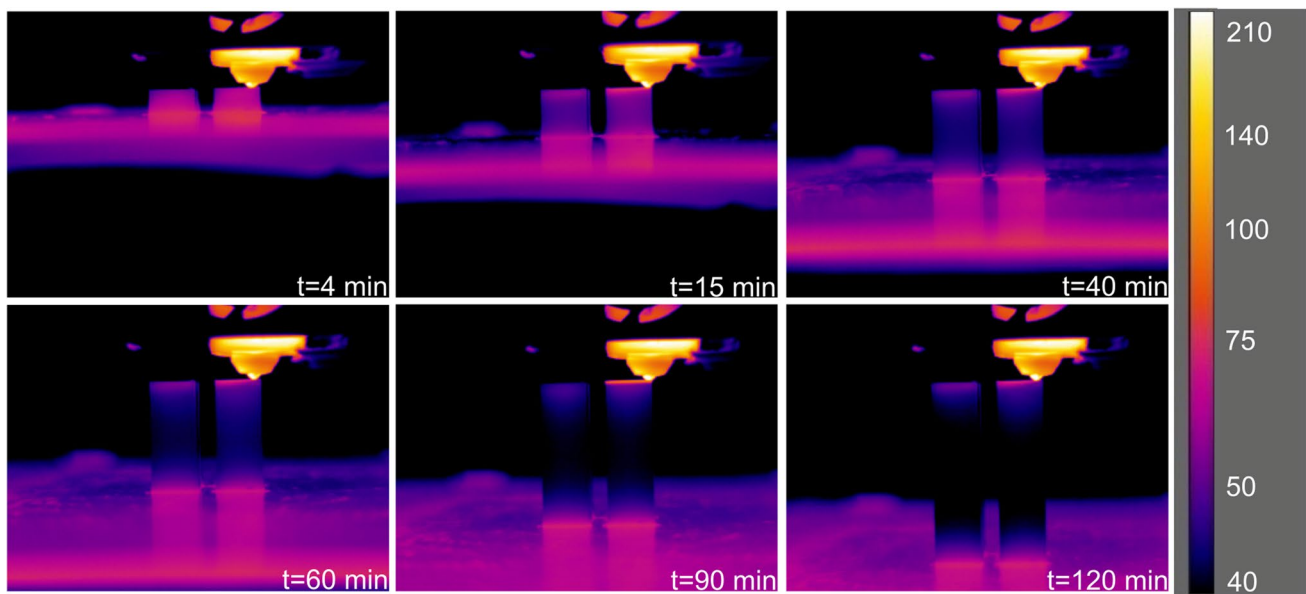


Fig. 12 IR maps recorded at different deposition times during 3D printing of four samples (two samples are behind the shown ones)

Further analysis was conducted to assess temperature variations within the actual layer. A fixed point (region of interest) was strategically placed at the center of the layer to monitor temperature fluctuations. As illustrated in Fig. 14a–c, the temperature exhibits a periodic trend corresponding to the nozzle's motion along the layer. Notably, when the nozzle passes through the ROI, the temperature reaches a peak and quickly decreases.

Comparing the temperature data collected under the three deposition conditions, it is evident that the average temperature of the actual layer varies. The average temperature for direct printing of a single sample was 93 °C, while it was 56 °C for direct printing of four samples in parallel. In contrast, the average temperature for the larger component was 43 °C. This variance can be attributed to the significantly smaller dimensions of the layers in the plate sample, which

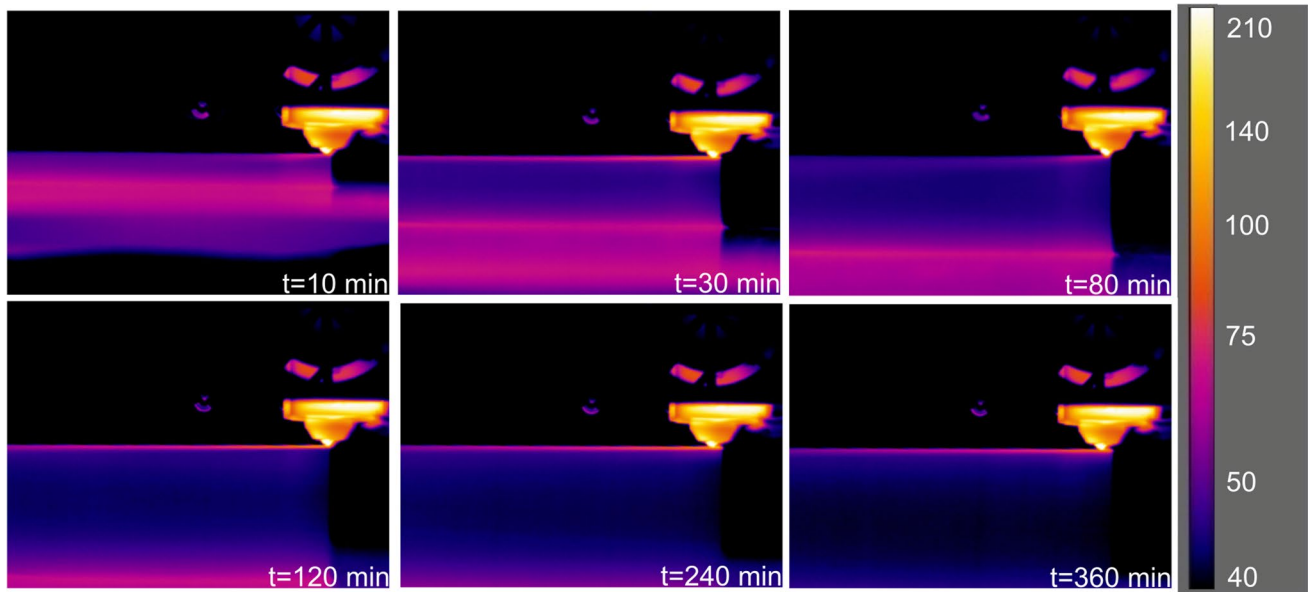


Fig. 13 IR maps recorded at different deposition times during 3D printing of the plate

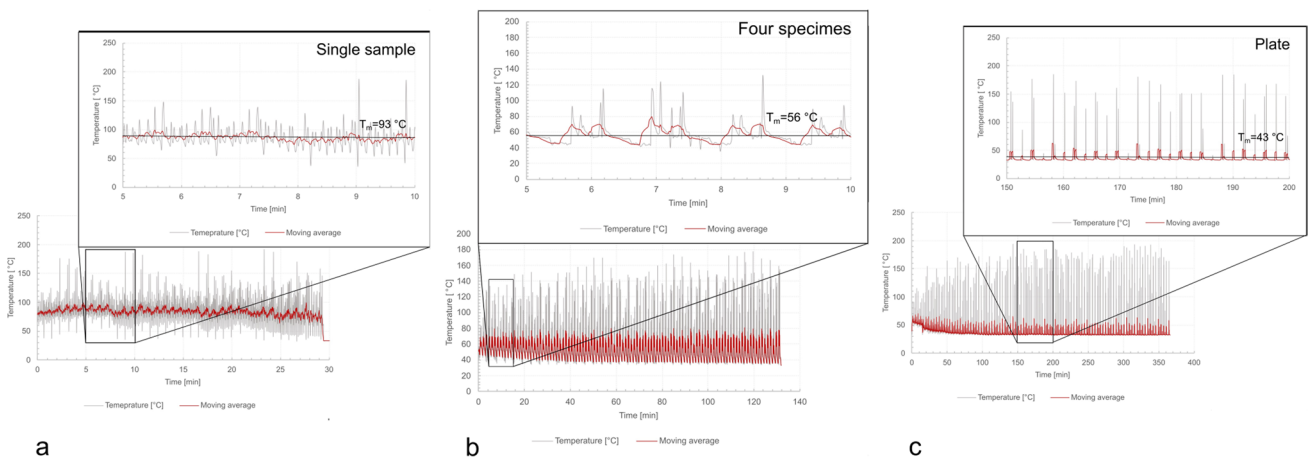


Fig. 14 Thermal history measured at the actual printing layer during the sample deposition using three strategies: **a** direct printing of one sample, **b** direct printing of four samples, and **c** printing of a plate

are nearly six times smaller. Therefore, it is apparent that the direct printing of a single sample, or even four samples in parallel, introduces more significant artifacts compared to plate printing, potentially impacting intermolecular diffusion, entanglement, and crystallinity.

4 Discussion

Additive manufacturing technologies are rapidly evolving from a rapid prototyping niche to a suitable solution for producing customized components, small batches, and even unique components manufacturing. So far,

applications of AM processes in fields such as biomedical and aerospace are growing significantly. This demands a deep understanding of the AM components' behavior and physical and mechanical properties [42]. For example, precise knowledge of the density and its engineering is required in the biomedical field for greater prosthesis integration. Similarly, the accurate identification of the mechanical behavior of the components is mandatory. Besides, unreliable characterization procedures may lead to underestimation or overestimation of the mechanical properties. This may lead to oversized structures in aerospace components, which would tremendously increase the space mission cost (the cost for getting a kilogram

of material in orbit is 5–10 k€). On the other hand, overestimation would lead to undersizing of the component with possible failure without the possibility of maintenance. These events make even more demanding the need for accurate characterization of these components and the definition of a reliable procedure.

Among AM processes, material extrusion is gaining great attention from both biomedical and aerospace fields because of the possibility of producing finished components with complex shapes made by biocompatible or high-strength-to-weight materials. The simplicity of the process, scalability, and opportunity to embed functionalizing fillers (such as reinforcing fibers, an electrically conductive filler) also contribute to attracting attention from both biomedical and aerospace fields.

The present investigation identified different causes of artifacts produced during direct sample printing. These included different thermal histories, (edge) regions where the deposition direction is inverted, rounded edges of the samples, and contact with the building plate shown in directly printed samples and determine different mechanical behavior from that of a larger component. These artifacts also add to the possible bad adhesion between the internal infill and the external shells, which should be avoided during mechanical characterization. The main artifacts introduced in the directly printed samples are depicted in Fig. 15.

In the present study, external shells were not printed, and only the internal infill was characterized. Nevertheless, the artifacts introduced by direct printing determined

significant differences in the measurements performed on directly printed samples and those extracted from a larger component. Table 4 summarizes the main differences in the properties measured on directly printed and extracted samples. As can be inferred, such differences greatly depend on the direction of the sample.

Figure 10 depicts schematically a sample printed under V1 conditions. As can be inferred, since the dimensions of the sample along the deposition path are relatively small (the edge is 12 mm long), the deposition conditions and especially the extruder speed are strongly uneven along the deposition path. Indeed, since the need for acceleration and deceleration ramps, only a small part of the path is effectively deposited under predefined steady-state speed. Therefore, the characteristics of the sample are greatly variable along the deposition path. This indicates that V1 samples suffer from edge effects. On the other hand, the samples “extracted” from the plate, as those of V2 type, are cut from an almost homogeneous region where the extruder speed is constant and equal to that prescribed. Consequently, V1 samples showed lower density and mechanical properties as the larger component. Thus, assuming the characteristics retrieved from direct printing sample testing would result in an underestimation of the final weight and oversizing of the component.

In the samples printed horizontally with filaments deposited transversely to the loading direction (H1), a negligible density difference was found compared to extracted samples (H3). On the other hand, an extremely lower Young’s

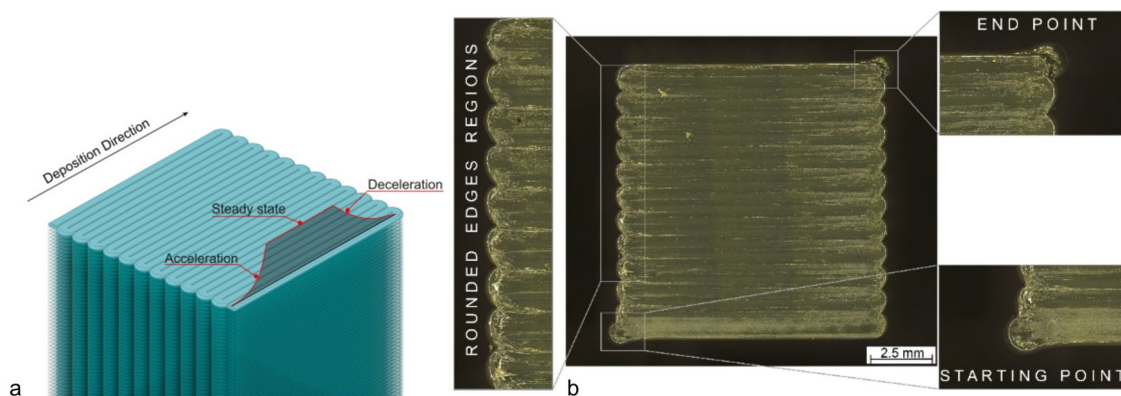


Fig. 15 Schematic of the deposition of directly printed vertical samples (V1 type) (a) with a zoom on main artifacts in directly printed samples (b)

Table 4 Difference of the density and mechanical behavior of samples made by direct printing (V1, H1, and HL1) and extraction method (V2, H3, and H2)

	Δ		
	Density	Young’s modulus	Yield strength
Vertical ($V_1 - V_2$)/ V_1	-5.3%	-10%	-12%
Horizontal-transverse ($H_1 - H_3$)/ H_1	0.6%	-29%	-3%
Horizontal-longitudinal ($HL_1 - H_2$)/ HL_1	3%	2%	18%

modulus was measured (29% lower). This difference was due to the shorter deposition path, which led to a different thermal history and a great edge effect. Finally, in samples printed horizontally with filaments arranged along the loading direction, the directly printed samples HL1 showed much higher yield strength values than the extracted samples H2. This was due to the large portion of samples HL1 in contact with the building plate. Such high values of yield strength were also observed in H4 samples. This confirms the strong influence of the densification occurring near the build platform on the yield strength. Similar results are in good agreement with the experimental findings concerning indentation tests performed on samples on the build platform face and the opposite one, as reported in [37].

All the previous comparisons indicate that, although direct printing of the samples by MatExt shows unquestionable advantages in terms of reduced efforts, time, and cost of manufacturing, it provides results that tend to underestimate or overestimate the mechanical properties of the deposition strategy. Such differences are certainly due to the acceleration/deceleration speed ramps that lead to uneven deposition conditions during the direct printing approach. In addition, this strategy is also affected by the rounding edges that further introduce significant artifacts in the geometry of the samples.

According to the findings discovered in the present investigation, some main considerations can be drawn:

- During the characterization of the samples, external layers should be avoided to avoid the issue of bad overlapping between the external shells and infill. These mainly alter the evaluation of the density and the effective cross-section (and consequently the mechanical properties of the samples).
- Direct printing of the samples should be used only for comparative purposes. Consequently, the adoption of directly printed samples should be limited to optimizing deposition conditions.
- Direct printing should be avoided for precise characterization aimed at determining the real mechanical characteristics of the samples, which should be used for mechanical simulation purposes of the component. In this case, sample extraction should be used instead.

The study provides a critical examination of how different manufacturing procedures can significantly impact the characterization of material extrusion (MatExt) components. This exploration of deposition strategies contributes to a deeper understanding of the complexities involved in additive manufacturing.

- The research highlights the necessity of considering sample dimensions when qualifying MatExt com-

ponents. This insight underscores the importance of robust qualification protocols that account for variations in sample size, ensuring representative results.

- A detailed analysis of thermal imaging was conducted, reaffirming the existence of distinct thermal histories during material deposition. This serves as valuable evidence to support our findings regarding the effects of different manufacturing approaches.

However, the study utilized a fixed set of process parameters, which might limit the generalizability of our findings. The influence of processing conditions, such as deposition speed, was not explored comprehensively. Future investigations should encompass a wider range of printing parameters to provide a more holistic perspective on their effects. While the study focused on the effects of different deposition paths on components, other printing parameters' impacts, like nozzle temperature and layer height, were not extensively examined. A more comprehensive exploration of these parameters could lead to a more nuanced understanding of their influence.

The main findings align with prior research that has highlighted the sensitivity of material extrusion processes to various parameters [46]. However, our study delves deeper into the specific influence of manufacturing protocols, expanding on the existing body of knowledge.

To address the limitation of fixed process parameters, future studies should encompass a broader spectrum of printing conditions. This includes variations in deposition speed, nozzle temperature, and layer height. Understanding how these parameters interact and influence artifacts and mechanical properties is essential for advancing the field. Developing more comprehensive qualification protocols that consider sample dimensions as a critical factor will contribute to more accurate representations of MatExt components. This is particularly crucial as the technology finds broader industrial applications.

Exploring the influence of different loading conditions, such as tensile, bending, and shearing, on components manufactured with various protocols can provide insights into the versatility and limitations of MatExt parts in real-world applications. Such investigations will be vital for tailoring MatExt components to specific industry needs.

5 Conclusions

In this study, the implications of varying manufacturing procedures on the characterization of components produced through material extrusion were explored. By investigating two distinct approaches—direct sample printing and sample extraction from larger components—we have unveiled key

insights that hold considerable promise for future research and practical applications in the field.

The research has illuminated the following overarching insights:

- The direct printing of samples introduced various artifacts, including alterations in thermal history, regions with inverted deposition directions, the formation of rounded sample edges, and interactions with the building platform.
- These differences in deposition paths under direct sample printing had a profound impact on the mechanical behavior of the components. Vertical samples produced via direct printing exhibited reduced density (– 5.3%), decreased Young’s modulus (– 10%), and lower yield strength (– 12%) when compared to their extracted counterparts.
- For horizontal samples with filaments oriented perpendicular to the loading direction, there was a notable underestimation of Young’s modulus (– 29%). Although these samples showed similar density (on average, 0.6% higher than the extracted samples), their yield strength was lower by – 3%.
- Conversely, horizontal samples with filaments aligned along the loading direction displayed higher density (+ 3%), increased Young’s modulus (+ 2%), and significantly elevated yield strength (+ 18%) compared to the extracted samples.

These findings collectively underscore the critical importance of selecting an appropriate manufacturing protocol in material extrusion processes. As we look ahead, this research not only enhances our understanding of the nuanced effects of manufacturing techniques but also paves the way for the development of tailored approaches that can optimize the properties of printed components. Future work may explore how these insights can be leveraged to improve the reliability and precision of material extrusion processes, ultimately advancing their applications across diverse industries.

Acknowledgements The authors would like to thank the contribution of Eng. Martina Ficcadenti for her contribution during the experimental tests.

Author contribution All the authors contributed to the design and implementation of the research, to the analysis of the results, and to the writing of the manuscript.

Funding Open access funding provided by Università degli Studi dell’Aquila within the CRUI-CARE Agreement.

Data availability The data supporting this study’s findings are available from the corresponding author, Francesco Lambiase, upon reasonable request.

Declarations

Conflict of interest The authors declare no competing interests.

Open Access This article is licensed under a Creative Commons Attribution 4.0 International License, which permits use, sharing, adaptation, distribution and reproduction in any medium or format, as long as you give appropriate credit to the original author(s) and the source, provide a link to the Creative Commons licence, and indicate if changes were made. The images or other third party material in this article are included in the article’s Creative Commons licence, unless indicated otherwise in a credit line to the material. If material is not included in the article’s Creative Commons licence and your intended use is not permitted by statutory regulation or exceeds the permitted use, you will need to obtain permission directly from the copyright holder. To view a copy of this licence, visit <http://creativecommons.org/licenses/by/4.0/>.

References

1. Perez-Mananes R et al (2021) Application of 3D printing and distributed manufacturing during the first-wave of COVID-19 pandemic. Our experience at a third-level university hospital. *3D Print Med* 7(1):7
2. Durão LFCS et al (2016) Distributed manufacturing of spare parts based on additive manufacturing: use cases and technical aspects. *Procedia CIRP* 57:704–709
3. Wittbrodt BT et al (2013) Life-cycle economic analysis of distributed manufacturing with open-source 3-D printers. *Mechatronics* 23(6):713–726
4. Berretta S et al (2017) Fused deposition modelling of high temperature polymers: exploring CNT PEEK composites. *Polym Testing* 63:251–262
5. Rinaldi M et al (2018) Additive layer manufacturing of poly (ether ether ketone) via FDM. *Compos B Eng* 145:162–172
6. Geng P et al (2019) Effects of extrusion speed and printing speed on the 3D printing stability of extruded PEEK filament. *J Manuf Process* 37:266–273
7. Zanjanijam AR, et al (2020) Fused filament fabrication of PEEK: a review of process-structure-property relationships. *Polymers (Basel)* 12(8):1665
8. Zhao Y et al (2020) Mechanical characterization of biocompatible PEEK by FDM. *J Manuf Process* 56:28–42
9. Dua R, et al (2021) Applications of 3D-printed PEEK via fused filament fabrication: a systematic review. *Polymers* 13(22):4046
10. Fischer M, Schöppner V (2017) Fatigue behavior of FDM parts manufactured with Ultem 9085. *Jom* 69(3):563–568
11. Zaldivar RJ et al (2017) Influence of processing and orientation print effects on the mechanical and thermal behavior of 3D-printed ULTEM® 9085 material. *Addit Manuf* 13:71–80
12. Cicala G, et al (2018) Comparison of Ultem 9085 used in fused deposition modelling (FDM) with polyetherimide blends. *Materials (Basel)* 11(2):285
13. Gebisa AW, Lemu HG (2018) Investigating effects of fused-deposition modeling (FDM) processing parameters on flexural properties of ULTEM 9085 using designed experiment. *Materials* 11(4):500
14. Wu H et al (2018) Multi-functional ULTEM™ 1010 composite filaments for additive manufacturing using fused filament fabrication (FFF). *Addit Manuf* 24:298–306
15. Chueca de Bruijn A, Gómez-Gras G, Pérez MA (2020) Mechanical study on the impact of an effective solvent support-removal

- methodology for FDM Ultem 9085 parts. *Polym Test* 85(4):106433
16. McLouth TD et al (2021) Enhancement of FDM ULTEM® 9085 bond strength via atmospheric plasma treatment. *J Manuf Process* 66:179–188
 17. Prechtel A et al (2020) Comparison of various 3D printed and milled PAEK materials: effect of printing direction and artificial aging on Martens parameters. *Dent Mater* 36(2):197–209
 18. Garcia-Leiner M et al (2021) Characterization of polyaryletherketone (PAEK) filaments and printed parts produced by extrusion-based additive manufacturing. *Polym Int* 70(8):1128–1136
 19. Luke SS et al (2021) Effect of fiber content and fiber orientation on mechanical behavior of fused filament fabricated continuous-glass-fiber-reinforced nylon. *Rapid Prototyp J* 27(7):1346–1354
 20. Brounstein Z, Yeager CM, Labouriau A (2021) Development of antimicrobial PLA composites for fused filament fabrication. *Polymers* 13(4):580
 21. Angelopoulos PM, Samouhos M, Taxiarchou M (2021) Functional fillers in composite filaments for fused filament fabrication; a review. *Mater Today: Proc* 37:4031–4043
 22. Zhang X, Fan W, Liu T (2020) Fused deposition modeling 3D printing of polyamide-based composites and its applications. *Compos Commun* 21:100413
 23. Penumakala PK, Santo J, Thomas A (2020) A critical review on the fused deposition modeling of thermoplastic polymer composites. *Compos B Eng* 201:108336
 24. Hu C, Qin Q-H (2020) Advances in fused deposition modeling of discontinuous fiber/polymer composites. *Curr Opin Solid State Mater Sci* 24(5):100867
 25. Dickson AN, Abourayana HM, Dowling DP (2020) 3D printing of fibre-reinforced thermoplastic composites using fused filament fabrication—a review. *Polymers* 12(10):2188
 26. Kechagias J, Chaidas D (2023) Fused filament fabrication parameter adjustments for sustainable 3D printing. *Mater Manuf Processes* 38(8):933–940
 27. Ko YS et al (2019) Improving the filament weld-strength of fused filament fabrication products through improved interdiffusion. *Addit Manuf* 29:100815
 28. Yi N et al (2021) Slow and fast crystallising poly aryl ether ketones (PAEKs) in 3D printing: crystallisation kinetics, morphology, and mechanical properties. *Addit Manuf* 39:101843
 29. Cao D et al (2023) Bending and shear improvements in 3D-printed core sandwich composites through modification of resin uptake in the skin/core interphase region. *Compos B Eng* 264:110912
 30. Srinivas V et al (2020) Promotion of molecular diffusion and/or crystallization in fused deposition modeled poly (lactide) welds. *Polymer* 202:122637
 31. Yin J et al (2018) Interfacial bonding during multi-material fused deposition modeling (FDM) process due to inter-molecular diffusion. *Mater Des* 150:104–112
 32. Özen A et al (2021) Exploring the role of manufacturing parameters on microstructure and mechanical properties in fused deposition modeling (FDM) using PETG. *Appl Compos Mater* 28(6):1799–1828
 33. Zhang R et al (2018) Aging-dependent strain localization in amorphous glassy polymers: from necking to shear banding. *Int J Solids Struct* 146:203–213
 34. Rodríguez-Panes A, Claver J, Camacho AM (2018) The influence of manufacturing parameters on the mechanical behaviour of PLA and ABS pieces manufactured by FDM: a comparative analysis. *Materials* 11(8):1333
 35. Dawoud M, Taha I, Ebeid SJ (2016) Mechanical behaviour of ABS: an experimental study using FDM and injection moulding techniques. *J Manuf Process* 21:39–45
 36. Nayak PK, Sahu AK, Mahapatra SS (2020) Effect of process parameters on the mechanical behavior of FDM and DMLS build parts. *Mater Today: Proc* 22:1443–1451
 37. Lambiase F, Scipioni SI, Paoletti A (2023) Mechanical characterization of FDM parts through instrumented flat indentation. *Int J Adv Manuf Technol* 125(9–10):4201–4211
 38. Lambiase F, Scipioni SI, Paoletti A (2022) Determination of local density in components made by fused deposition modeling through indentation test. *Int J Adv Manuf Technol* 122(3–4):1467–1478
 39. Dua R et al (2021) Applications of 3d-printed peek via fused filament fabrication: a systematic review. *Polymers* 13(22):4046
 40. Boparai KS, Singh R, Singh H (2016) Development of rapid tooling using fused deposition modeling: a review. *Rapid Prototyp J* 22(2):281–299
 41. Ai J-R, Vogt BD (2022) Size and print path effects on mechanical properties of material extrusion 3D printed plastics. *Prog Addit Manuf* 7(5):1009–1021
 42. Stamopoulos AG, Scipioni SI, Lambiase F (2023) Experimental characterization of the interlayer fracture toughness of FDM components. *Compos Struct* 320:117213
 43. Lambiase F, et al (2023) Influence of the deposition pattern on the interlayer fracture toughness of FDM components. *Int J Adv Manuf Technol* 128:4269–4281
 44. Kechagias J et al (2023) A multi-parametric process evaluation of the mechanical response of PLA in FFF 3D printing. *Mater Manuf Processes* 38(8):941–953
 45. Bartolai J, Simpson TW, Xie R (2018) Predicting strength of additively manufactured thermoplastic polymer parts produced using material extrusion. *Rapid Prototyp J* 24(2):321–332
 46. Gonabadi H, Yadav A, Bull S (2020) The effect of processing parameters on the mechanical characteristics of PLA produced by a 3D FFF printer. *Int J Adv Manuf Technol* 111:695–709

Publisher's Note Springer Nature remains neutral with regard to jurisdictional claims in published maps and institutional affiliations.